

Transition from active motion to anomalous diffusion for *Bacillus subtilis* confined in hydrogel matrices

Gavino Bassu^{a,b}, Marco Laurati^{a,b,*}, Emiliano Fratini^{a,b}

^a Department of Chemistry "Ugo Schiff", Via della Lastruccia 3, Sesto Fiorentino 50019, Italy

^b Consorzio per lo Sviluppo dei Sistemi a Grande Interfase (CSGI), Via della Lastruccia 3, Sesto Fiorentino 50019, Italy

ARTICLE INFO

Keywords:

Micro-confinement
Bacillus subtilis
 Bacterial motility
 Single-trajectory analysis
 Poly(ethylene glycol) hydrogels

ABSTRACT

We investigate the motility of *B. subtilis* under different degrees of confinement induced by transparent porous hydrogels. The dynamical behavior of the bacteria at short times is linked to characteristic parameters describing the hydrogel porosity. Mean squared displacements (MSDs) reveal that the run-and-tumble dynamics of unconfined *B. subtilis* progressively turns into sub-diffusive motion with increasing confinement. Correspondingly, the median instantaneous velocity of bacteria decreases and becomes more narrowly distributed, while the reorientation rate increases and reaches a plateau value. Analyzing single-trajectories, we show that the average dynamical behavior is the result of complex displacements, in which active, diffusive and sub-diffusive segments coexist. For small and moderate confinements, the number of active segments reduces, while the diffusive and sub-diffusive segments increase. The alternation of sub-diffusion, diffusion and active motion along the same trajectory can be described as a hopping and trapping motion, in which hopping events correspond to displacements with an instantaneous velocity exceeding the corresponding mean value along a trajectory. Different from previous observations, escape from local trapping occurs for *B. subtilis* through active runs but also diffusion. Interestingly, the contribution of diffusion is maximum at intermediate confinements. At sufficiently long times transport coefficients estimated from the experimental MSDs under different degrees of confinement can be reproduced using a recently proposed hopping and trapping model. Finally, we propose a quantitative relationship linking the median velocity of confined and unconfined bacteria through the characteristic confinement length of the hydrogel matrix. Our work provides new insights for the bacterial motility in complex media that mimic natural environments and are relevant to important problems like sterilization, water purification, biofilm formation, membrane permeation and bacteria separation.

1. Introduction

Motile bacteria are ubiquitous in micro-environments like animal or plant tissue, soil, waste, granulated, and porous materials, and play a fundamental role in health (infectious diseases[1,2], nutrition[3], pharmaceuticals[4]), agriculture[5,6], environmental science[7,8], and industrial activities[9]. Bacterial motility is associated with specific propelling mechanisms[10] that allow them to run, reorient and diffuse in a multitude of environments with narrow porosity comparable in size with the bacterial cell. The most commonly observed propulsion mechanism is the flagellum-based motion. This is governed by the number of flagella and their distribution on the bacterial cell that, coupled with the bacterial morphology (i.e. coccus, bacillus, vibrio), determine different motility modes (i.e. run-and-tumble, run-and-flick

[11], and various motility behaviors (e.g., swimming, tumbling, and swarming)[10,12]. The full hydrodynamic description of the flagella-induced propulsion has been previously reported[13]. For rod-shaped swimming bacteria, the run-and-tumble motility mode is the most common. It consists in the repetition of straight-line running processes (*run*) in which bacteria propel themselves through the rotation of bundled flagella, and rapid reorientations (*tumble*) in which bacteria unbundle the flagella allowing a change of direction in response to stimuli. For times longer than the duration of a run, the run-and-tumble motion becomes diffusive, with a translational diffusion coefficient given by $1/3\langle V_r \rangle \langle L_r \rangle$ [14], (where $\langle V_r \rangle$ and $\langle L_r \rangle$ define the mean speed and length of the run, respectively).

The effects of the bacteria environment on this type of motility has been studied in detail during the last years. In particular the effect of the

* Corresponding author at: Department of Chemistry "Ugo Schiff", Via della Lastruccia 3, Sesto Fiorentino 50019, Italy.

E-mail address: marco.laurati@unifi.it (M. Laurati).

<https://doi.org/10.1016/j.colsurfb.2024.113797>

Received 2 August 2023; Received in revised form 6 December 2023; Accepted 11 February 2024

Available online 15 February 2024

0927-7765/© 2024 The Authors. Published by Elsevier B.V. This is an open access article under the CC BY-NC-ND license (<http://creativecommons.org/licenses/by-nc-nd/4.0/>).

vicinity of surfaces was investigated using traditional flat plate cultures [15–18]. Interestingly, it was found that the presence of a surface significantly affects the swimming motion leading to transient accumulation of bacteria close to the surface due to hydrodynamic-induced attractions [17], noise effects [18] and persistent motion [19,20], even in the absence of any additional physical constraint. Recent studies in channel confinement show that an important role is also played by a large variation in the run-time duration [21]. While traditional growth media allow direct observation of both growing colonies and single-cell motion, they are not representative of the natural habitats of microorganisms (i.e., heterogeneous 3D micrometric porous media) and of the surfaces with which bacteria interact. A first step in the direction of exploring 3D confinement effects that mimic those of natural habitats was the investigation of motility in confining microfluidic channels [22–25,26]. These studies revealed the importance of cell-surface interactions, showing that bacteria swim at significantly higher speed near the surface of the microfluidic channel [23,25]. Furthermore, the swimming path and speed are significantly affected by the channel's diameter: narrowing the confining channel results in a dramatic reduction of the swimming speed and of the reorientation capacity of the bacteria. Increasing the complexity of the confining structure, moving from linear or comb channels to a microfluidic labyrinth, dramatically affects the motility properties of swimming bacteria. Despite the numerous interesting findings, microfluidic conditions are still far from natural conditions, where bacteria swim in multiple interconnected channels of different sizes within 3D porous media.

Efforts in approaching such complex conditions include a phenomenological analysis of bacterial motions in granular media [27], and numerical simulations of model porous media [28,29], that focused on the effects of interactions of bacteria with solid surfaces. These interactions significantly influence bacterial reorientation [26,29,30]. Major advances were achieved recently through the development of transparent heterogeneous matrices [31–33] to directly observe and study bacterial migration in disordered highly confining 3D environments. As highlighted by Datta *et al.* in their works on *E. coli* [31,34], the motility in highly complex porous media, in which pore sizes become comparable to the bacteria body size, cannot be described in terms of the classic run-and-tumble model, even when the running length is replaced by the characteristic diameter of the pores [35,36]. The bacterial dynamics change qualitatively, being characterized by alternate trapping in tight or tortuous paths, and hopping out of them through active, directed runs. This led to a revisited model of diffusivity that provides good agreement with experimental observations. Some questions remained however opened. The first question is whether the qualitative change in the dynamics observed for *E. coli* is a general feature of confined motion of flagellated bacteria presenting run-and-tumble motility. In addition, the hopping and trapping model was used to describe the final diffusion of bacteria, that follows a regime of anomalous diffusion, in which the dynamics become progressively sub-diffusive with increasing degree of confinement. Whether this regime can be rationalized in terms of a qualitative change in the dynamics of single bacteria and how its extent and the eventual transition to diffusion depend on confinement remains unclear.

In this work, we address these open questions through a detailed single cell analysis of the dynamics of a different flagellated bacterium, *Bacillus subtilis*, a Gram-positive, non-pathogenic, rod-shaped soil bacterium that is recognized as a “universal cell factory” in the industrial production of enzymes, proteins, and other bio-products [37]. Thanks to its excellent physiological characteristics [38,39], an highly adaptable metabolism and its bio-film forming capacity, *B. subtilis* finds application in many fields of technology, from agriculture for the bio-fertilization of the soil to the development of biomaterials [40–43–46]. Despite this large number of attractive applications, *B. subtilis* remains far less studied than its Gram-negative counterpart, *E. coli*, and a clear explanation of the role of its transport properties on its beneficial effects was only partially explored [47]. To induce confinement we used

application-relevant, disordered 3D transparent hydrogels of polyethylene glycol with porosity that can be tuned at the micron scale [33]. Detailed characterization of the porosity was achieved through the analysis of volume image stacks of fluorescently labeled hydrogels. Through single-cell tracking applied to time series of confocal microscopy images, we analyzed the trajectories of hundreds to thousands individual bacteria (depending on confinement) confirming that also for *B. subtilis* the average mean squared displacements (MSD) show a progressive transition from active to sub-diffusive motion at short times with increasing the confinement length. This transition was associated to an increase in the reorientation rate and a decrease in the median instantaneous velocity of the bacteria. To understand the microscopic origin of the observed anomalous diffusion, we classified segments of bacterial trajectories as active, normal, and sub-diffusive under the different confinement conditions investigated. This classification showed that the anomalous diffusion regime and its dependence on confinement can be understood microscopically in terms of the population of active, diffusive and sub-diffusive trajectory segments that compose a single trajectory. While in unconfined conditions almost only active segments were observed, for the strongest confinement these almost disappeared in favor of sub-diffusive segments. We revealed in addition that sub-diffusive segments can be seen as trapping events, while active and diffusive segments as hopping events. Thus, different from what reported for *E. coli*, release from local trapping occurs through both diffusive and active motion. Finally, we show that at the longest time measured for the MSDs, the time-dependent diffusion coefficient presents values consistent with the hopping and trapping model, and that the average bacterial velocity in confinement can be expressed in terms of the unconfined velocity through the characteristic size of the confining pores.

2. Materials and methods

2.1. Chemicals

Poly(ethylene glycol) (PEG), molar weight 35000 g/mol (purity 99%), acryloyl chloride (purity 97%), and 2,2-Dimethoxy-2-phenylacetophenone (DMP) (purity 97%) were purchased from Merck. As reported in [48], the hydroxyl termini of PEG polymeric units were acrylated by a 4-fold molar excess of acryloyl chloride and triethylamine in 100 mL of dichloromethane under nitrogen atmosphere. The obtained poly(ethylene glycol) diacrylate (PEGDA) was precipitated in cold diethyl ether. The obtained white powders were dried and stored at -20°C until use.

Water solution of glutaraldehyde (5 wt%), *tert*-butanol solution of Osmium tetroxide (2.5 wt%) and Phosphate buffer saline pills were purchased from Sigma Aldrich. The fluorescent probes Rhodamine B (RhB) (purity $\geq 95\%$) and SYTO9 (from Live/Dead BacLight™), respectively from Sigma Aldrich and Thermo Fisher Scientific, were used to prepare the dye solutions following instructions provided by suppliers. Water was purified by a Millipore Milli-Q gradient system (resistivity $< 18 \text{ M}\Omega \cdot \text{cm}$).

2.2. Hydrogel preparation

Hydrogels' synthesis was carried out by radical photopolymerization of the acrylated polymeric units (PEGDA) in water solution. In order to obtain transparent polymeric networks with porosity in the range from 5 to 20 μm , an experimental procedure developed in previous studies was followed [33]. 10 μL of a DMP ethanol solution (0.2 g/mL) were added to the macro-monomer water-solutions and the mixtures were fluxed with nitrogen for 1 minute. The homogenized pre-reaction mixture was placed in demountable glass molds of 2 mm in thickness and completely polymerized under UV light (power = 55 W and $\lambda = 365 \text{ nm}$) overnight. After polymerization, the hydrogels were cut into squares of 1 cm side and kept in water until reaching

equilibrium, replacing the water every 24 hours. The swollen hydrogels were then freeze dried to induce porosity at the microscale by immersion in liquid nitrogen for 5 minutes and then dried at -55°C and 40 mtorr overnight. The ice crystals generated during the freezing process act as a porogen within the polymeric network. After the freeze-drying procedure, the gels were re-hydrated in MilliQ water for 48 hours. After lyophilization, the re-hydrated samples kept their elasticity and mechanical properties, showing a small loss of transparency. This however did not significantly affect the confocal microscopy measurements. The prepared gels were labeled with Rhodamine B to directly observe the porous structure during each experiment. Each gel was equilibrated in Rhodamine B solution for 72 hours. The hydrogels were named using the initial letter "P" followed by the monomer concentration in the pre-reaction mixture. Under this notation, the investigated hydrogels fall in the range from P10 to P25. Fig. S1 in the Supplementary Information (SI) evidences the effects of lyophilization on the hydrogel porosity: without the lyophilization step, compact gel structures were obtained.

2.3. Bacterial culture

Bacillus subtilis (*B. subtilis*) type strain DMS-10 was purchased from DMSZ (Germany). The bacterial pellet was reactivated following the supplier's instructions. Then the activated culture was diluted in fresh tryptic soy broth (TSB) to reach the optical density of approximately 1, measured at the wavelength of 600 nm (OD_{600}) with a Thermo Scientific NanoDrop OneC UV-Vis Spectrophotometer. An overnight culture of *B. subtilis* was prepared for each experiment by inoculation of one colony in 5 mL TSB at 32°C under agitation at 260 rpm. The stationary phase was confirmed thanks to the measure of OD_{600} of the bacterial dispersion at intervals of 30 minutes. To maximize the number of motile cells, the bacterial dispersion was diluted to $\text{OD}_{600} = 0.15$ in fresh TSB and kept at the growing conditions for 30 minutes. Direct visualization of the motile cells was performed by staining *B. subtilis*'s cells with SYTO9 directly on the activated dispersion. The dye solution was added to the bacterial dispersion to a final concentration of 10 vol% and kept under soft agitation for 15 minutes in the dark. The final bacterial dispersion was sufficiently diluted to minimize local gradients of oxygen or nutrient concentration and intercellular interactions throughout the entire media.

2.4. Characterization of the hydrogel porosity by confocal microscopy

Imaging of hydrogel volumes was carried out using a Leica TCS SP8 confocal microscope. Lab-Tek chambered coverglass with 1.0 borosilicate glass bottom were used as sample holders. A $63\times$ oil immersion objective with N.A. = 1.43 was used for all experiments. The rehydrated hydrogels were immersed in a solution of RhB for 72 hours to allow physical adsorption of the dye in the polymeric network. The fluorescent dye was excited with a laser having a wavelength of 561 nm, and the fluorescence emission was acquired using a highly efficient hybrid detector in the 600–700 nm range. The greater affinity of the fluorescent dye to the polymeric network ensures the direct observation of the porous network with good contrast between the labeled gels and the dye solution. Due to that, no washing cycles were required to remove the dye solution. 3D stacks of $1024 \times 1024 \times 40$ pixels³, corresponding to volumes of $90 \times 90 \times 40 \mu\text{m}^3$, were acquired. In order to extrapolate the morphological features of the porous networks, 3D stacks acquired by confocal microscopy were analyzed using MorphoLibJ, a library of mathematical methods for ImageJ[49]. The "Distance Transform Watershed" method was applied to the binary images to distinguish each pore allowing the extrapolation of the geometrical and morphological parameters.

2.5. Morphological characterization of bacteria by scanning electron microscopy

Morphological characterization of *B. subtilis* was performed by scanning electron microscopy (SEM). To fix the biological tissue, after overnight culture, 1 mL of the bacterial dispersion was centrifuged (1500 g for 10 min), suspended in 1 mL of 2.5 wt% glutaraldehyde solution, and incubated for 24 hours at 4°C in the dark. The bacterial suspension was washed with phosphate buffer 0.2 M solution (PBS) and then resuspended in 1 wt% osmium tetroxide PBS solution for 2 hours. Afterwards, the bacterial dispersion was washed twice with PBS. The sample was dehydrated in rising ethanol gradient 50, 70, and 95 vol% for 10 min and then 100 vol% for 1 min. Further dehydration was carried out with three washing steps of 30 s in acetone-ethanol solutions of 1:2, 1:1, 2:0 v/v respectively. Scanning electron microscopy (SEM) investigation on the metallized sample was performed using a FEG-SEM SIGMA (Carl Zeiss, Germany), at a working distance of 3 mm and with an acceleration potential of 2 kV.

2.6. Adsorption of bacteria within the hydrogels

Bacteria were adsorbed within the hydrogels by immersion of the gel in bacterial dispersion. To erase possible biases of different nutrient or oxygen concentrations, the hydrogels were previously equilibrated in fresh TSB culture overnight in sterile vials. In order to induce the desired adsorption within the polymeric network, 200 μL of the bacterial dispersion prepared in section 2.3 were gently placed in an 8-well Labtec sterile plate and then equilibrated hydrogels were then directly placed in contact with the bacterial dispersion and kept under soft agitation for 15 minutes in the dark. The bacterial penetration and proliferation were observed by 3D stacks acquired by confocal microscopy.

2.7. Tracking of bacterial motions

The motility of the bacteria was determined through confocal microscopy measurements in unconfined and confined conditions using the same instrumental setup described for the morphological characterization of the porous networks. Rhodamine B (hydrogel) and SYTO9 (bacteria) were excited with 561 nm and 488 nm lasers, respectively, while the fluorescence emissions were acquired using two highly efficient hybrid detectors in the 571–600 nm (hydrogel) and 498–550 nm (bacteria) ranges. Time-series of 2000 images of 512×512 pixels², which correspond to a sample area of $42 \times 42 \mu\text{m}^2$, were acquired in the bulk with a frame interval of 0.036 s. All measurements were conducted at room temperature. Image time-series of the diffusing bacteria were analyzed using Trackpy v0.50[50,51] to obtain particle locations and trajectories. The software allowed the correction of any background drift which might be due to large-scale flow or any microscope stage movement. The ensemble mean squared displacement (MSD) of all particles was computed using the "emsd" function in Trackpy. TrackMate and TrackClassifier, two Fiji plugins, were used in order to analyze single trajectories and their characteristic speeds, and to classify them into normal diffusion, sub-diffusion, confined diffusion, and directed/active motion[52–54]. In TrackMate the Difference of Gaussian ("DoG") detection algorithm was applied to automatically detect the bacteria in the acquired image time-series. The Linear Assignment Problem (LAP) particle-tracking algorithm[55] was selected to link the positions to form trajectories. The obtained trajectories were classified through TrajClassifier.

3. Results and discussion

3.1. Characterization of the porous networks

The morphological and geometrical characterization of the pores performed by confocal microscopy revealed a progressive reduction of

the pore size with the increase of PEG content. Fig. 1 shows exemplary 3D image stacks from fluorescently labeled gels. It is evident that the pores decrease in size with increasing PEG content (from (a) to (c)). The precise morphological characterization of the confining structures performed with MorphoLibJ (see Sec. 2.4 for more details) allowed the extrapolation of the pore volume fraction (Φ), defined as the sum of the pores' volumes divided by the total volume of the imaged portion of the

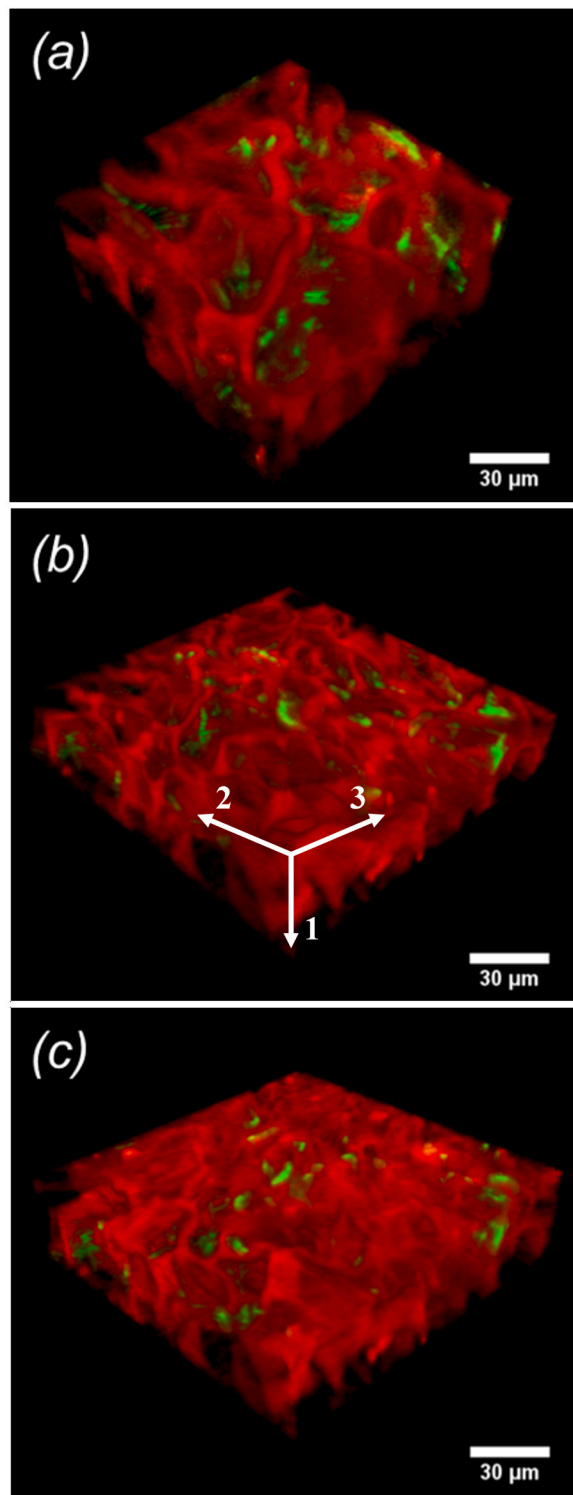


Fig. 1. Confocal microscopy image stacks of RhB labeled porous hydrogels (red) with increasing PEG content: (a) P10, (b) P16 and (c) P20. *B. subtilis* cells adsorbed within the hydrogels are labeled in green.

gel (V_{tot}):

$$\Phi = \frac{\sum_i V_{\text{pore}}^i}{V_{\text{tot}}} \quad (1)$$

where V_{pore}^i indicates the volume of pore i . Moreover, from the 2D sections of the stacks, the mean diameter of the equivalent circle for each detected object, $\langle d \rangle$, was extracted (mean values for each hydrogel are reported in Tab. S1 of the SI). These values were used to calculate the pore area fraction (α), defined as the total area of the pores in the investigated 2D plane normalized by the total area of the 2D plane:

$$\alpha = \frac{\sum_i A_{\text{pore}}^i}{A_{\text{tot}}} \quad (2)$$

where A_{pore}^i is the area of pore i . Finally, in order to assess the pore geometry and symmetry, after removing the pores on the edges the image stacks were analyzed to extract the three characteristic lengths of the ellipsoid that best fits within a pore, called R_1 , R_2 and R_3 (see Fig. 1b for the definition of the axes 1, 2 and 3).

Consistent with the qualitative discussion of Fig. 1, the mean diameter $\langle d \rangle$ obtained by the analysis of 2D slices (such as those in Fig. S4 of the SI) decreases from approximately $20 \mu\text{m}$ to $5 \mu\text{m}$ for a PEG content increase from 10 wt% to 25 wt% ($\langle d \rangle$ values reported in Tab. S1 of the SI). Exemplary 3D pore reconstructions obtained through MorpholibJ are reported in Fig. S1 of the SI. The pore volume fraction (Φ) decreases from 65% to 45% with increasing macro-monomer content from 10 to 20 wt%, and dramatically drops for larger PEG concentrations, reaching the value 4.5% for the sample with a PEG content of 25 wt% (Fig. S2 in the SI). These results indicate a qualitative change from a network structure with interconnected pores to a more compact structure with fewer and less interconnected pores when the PEG content becomes larger than 20 wt%. A comparable trend is obtained for the area fraction (Fig. S2 in the SI). The geometrical analysis of pore symmetry in terms of the ellipsoid axed R_1 , R_2 and R_3 revealed the presence of channel-like pores elongated in the 1 direction and with asymmetric sections in the 2–3 plane (see pore reconstructions in Fig. S1 of the SI). Overall, the analysis of the pore structure confirms the impact of the freeze-drying and the role of the ice-crystals as a porogen. [56,57].

3.2. Morphological characterization of the bacteria

The morphology and characteristic size of *B. subtilis* was investigated using SEM imaging. The fixation procedure preserved the delicate bacterial main structure from collapsing in the vacuum conditions of the SEM measurements. As shown in Fig. S3 of the SI the metallization process preserved the bacterial cells from biases allowing the clear observation of the bacterial main body. Consistent with the literature [58] the growth conditions produce well-defined cells of length $l_{\text{bacteria}} = 2.10 \pm 0.20 \mu\text{m}$ and width $w_{\text{bacteria}} = 0.60 \pm 0.05 \mu\text{m}$, with the error estimated on the basis of image analysis. Unfortunately, bacterial flagella could not be observed. Due to their intrinsic fragility, the flagella were damaged during the fixation and metallization steps.

3.3. Dynamics of bacteria

Thanks to the different labeling of the bacteria and the hydrogels, one can clearly observe in Fig. 1 that the *B. subtilis* bacteria were successfully absorbed in the bulk of the hydrogels. While in principle confocal microscopy would allow following the bacterial dynamics in 3D, at least for the unconfined bacterial dispersion the bacteria moved faster than the acquisition rate of image stacks. For this reason, we decided to investigate the dynamics in a 2D plane (2–3 plane, see Fig. 1b) in the bulk. Owing to the channel-like nature of the porosity, with the pore size in the 1 direction being much larger than that in the 2–3 plane, we can in any case assume that the major confinement effects

should be revealed by the study of the in-plane dynamics. Exemplary in-plane images of the bacteria confined in hydrogels of decreasing pore size are shown in Fig. S4 of the SI.

3.3.1. Mean squared displacements

The average bacterial mean squared displacements (MSD) were calculated from the trajectories determined using Trackpy according to the following expression:

$$\langle \Delta r^2(\tau) \rangle = \langle [x(t+\tau) - x(t)]^2 + [y(t+\tau) - y(t)]^2 \rangle_{i,t} \quad (3)$$

where x and y are the time-dependent coordinates of the centroid representing the diffusing bacteria and $\langle \rangle_{i,t}$ indicates an average over all bacteria i and all starting times of the trajectories extracted from an image time-series. τ is the lag-time between two positions of a particle along a trajectory. The average MSDs obtained for bacteria confined in hydrogels of different porosity are shown in Fig. 2a. To characterize the different degree of confinement, we introduce the confinement length ξ , defined as the ratio between the bacterial length and the average pore diameter:

$$\xi = \frac{l_{\text{bacteria}}}{\langle d \rangle} \quad (4)$$

Values of ξ for different confining conditions are reported in Tab. S1

of the SI.

As it can be clearly seen, the MSD progressively decreases with decreasing the average pore diameter (increasing confinement length). To assess the nature of the bacterial motion, we fit the time dependence of the MSDs using the following expression:

$$\langle \Delta r^2(\tau) \rangle = 4\langle K \rangle \tau^n \quad (5)$$

where $\langle K \rangle$ is an average transport coefficient while the exponent n is related to the nature of the motion. Note that the units of $\langle K \rangle$ are $\mu\text{m}^2/\text{s}^n$ and change depending on n for the different samples. For $n = 1$ the motion is diffusive, while for n smaller than 1 it becomes sub-diffusive. In the case of active motion, at short times n becomes greater than 1 highlighting super-diffusive motion. Consistent with expectations, unconfined bacteria exhibit at short times run-and-tumble motion, as also evidenced by single trajectories (Fig. 2b, left panel). This is confirmed by the super-diffusive exponent $n \approx 1.70$ [59,60] obtained by fitting Eq. (5) to the experimental MSD. The fit also yields the transport coefficient $\langle K \rangle = 26.28 \mu\text{m}^2/\text{s}^{1.70}$. Fitting instead the last points of the MSD for $\tau > 0.8$ s, where the slope changes indicating onset of randomization and diffusion, using $\langle \Delta r^2(\tau) \rangle = 4\langle D \rangle \tau$, we obtain $\langle D \rangle \approx 20.05 \mu\text{m}^2/\text{s}$, that agrees well with previous findings [59] even if the number of points used for the fit is small.

For the confined cases, following theoretical models of anomalous

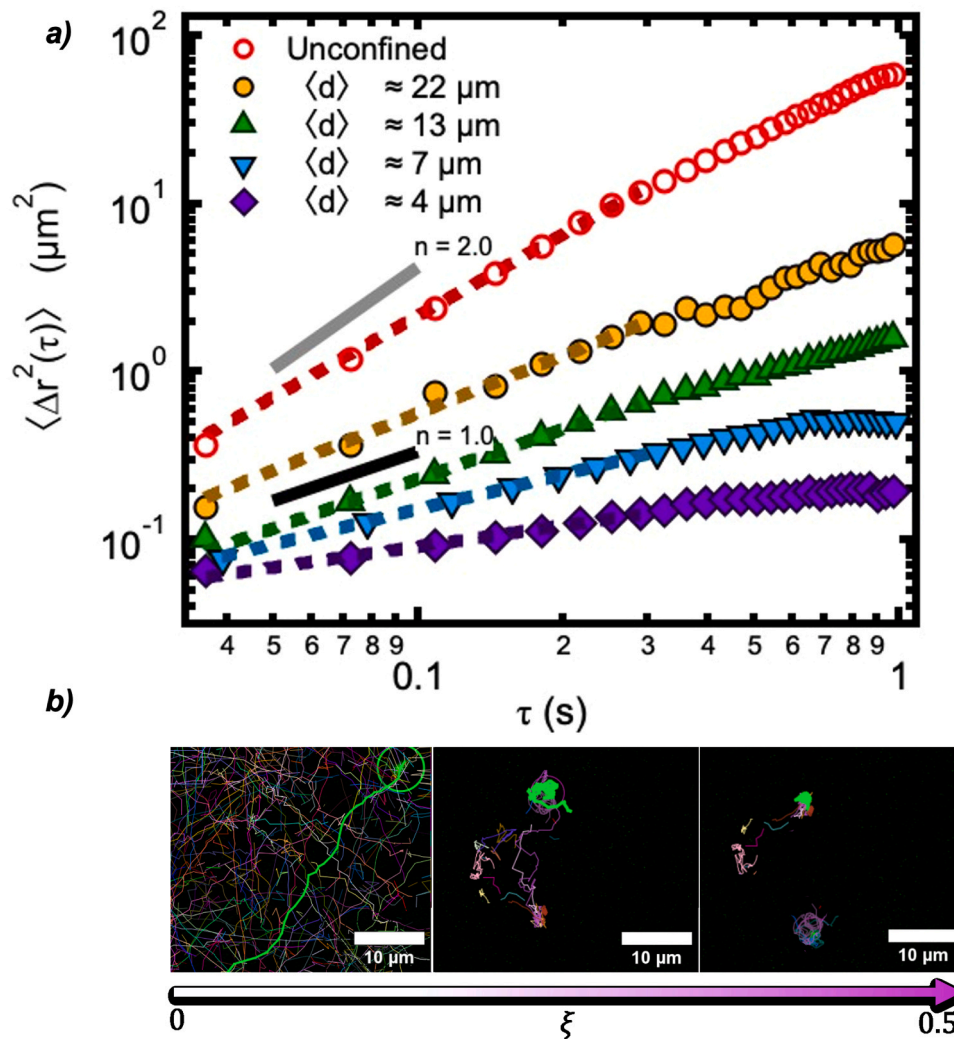


Fig. 2. (a) Mean Squared Displacements of bacteria in unconfined conditions (empty markers) and loaded in the different porous hydrogels (full markers). Dotted lines represent fits according to Eq. (5). (b) Exemplary single trajectories obtained from TrackMate (highlighted in green), for three different values of the confinement length increasing from 0 to 0.5. Additional lines correspond to other bacterial trajectories.

diffusion, like Continuous Time Random Walk or Scaled Brownian Motion[61,62]. we introduce the time-dependent diffusion coefficient, defined as $D(\tau) = nK\tau^{n-1}$ and having the same dimensions of $\mu\text{m}^2/\text{s}$ for all samples. In order to qualitatively compare the dynamics of samples under different degrees of confinement we calculate then $D(\tau = 1\text{s})$, the longest time at which the MSD was determined. For the less confining gel, with a pore diameter of approximately $22\ \mu\text{m}$, the MSD presents an approximately diffusive behavior with $n = 1.05$, while $D(\tau = 1\text{s}) = 1.98\ \mu\text{m}^2/\text{s}$. i.e. about an order of magnitude smaller than $\langle D \rangle$ of the unconfined bacteria. The qualitative change from active motion to diffusion is visible in the single particle trajectories (Fig. 2b, central panel). Further increasing the confinement sub-diffusion with increasingly smaller exponent n and transport $D(\tau = 1\text{s})$ is observed. We also note that the sub-diffusive behavior spans the whole time range and for the smallest pore diameter indications of localization are found at long times, where the MSD seems to approach a plateau value (Fig. 2a). An exemplary trajectory showing localization is reported in Fig. 2b, right panel. All values of n and $D(\tau = 1\text{s})$ are reported in Tab. S1 of the SI. Note that for the smallest pore size $D(\tau = 1\text{s}) \approx 0.03\ \mu\text{m}^2/\text{s}$ is almost three orders of magnitude smaller than $\langle D \rangle$ in the unconfined case, and $n \approx 0.43$.

From the results on the average MSDs we can conclude that increasing confinement in a random porous matrix induces a progressive crossover from run-and-tumble active motion to average diffusive motion and then average sub-diffusive motion at short times. Different from previous investigations on *E. coli*[31,34], we do not find that all MSDs present a comparable slope at the shortest times. Differences in the confined motility of *E. coli* and *B. subtilis* have been reported earlier in microfluidic confinement[22] and have been associated to the different capability to deform of the two bacteria. Consistent with other studies [63], pores an order of magnitude larger than the bacteria's length already affect bacterial motility. We additionally determined the distributions of particle displacements under all confinement conditions (see SI, Fig. S5). Consistent with the MSDs, their width reduces with increasing confinement. Additionally, non-Gaussian tails characteristic of localization and sub-diffusive dynamics, are observed for all confinement conditions. Interestingly, the tails are more pronounced for smaller degree of confinement. This is confirmed by the calculation of the non-Gaussian parameter α_2 [64] reported in Fig. S6 for three different confinement conditions. As it can be seen, deviations from Gaussian behavior are particularly pronounced for the smallest confinement, even though the corresponding MSD shows an approximately diffusive behavior in the same delay-time window. This might be the result of the heterogeneous nature of bacterial trajectories under confinement, that will be analyzed in detail in the following sections.

The characteristic motility parameters were then related to the morphological parameters of the porous network. Fig. 3 shows the dramatic reduction of $D(\tau = 1\text{s})$ with increasing ξ , which can be described as an exponential decay $A\exp(-B\xi)$ with $B \approx 24.0$. The reduction of n as a function of ξ can be also described by an exponential decay with $B \approx 6.5$. It is interesting to note that even for the less confining polymer matrix, the average dynamical behavior changes from super-diffusive to diffusive, as indicated by $n \approx 1$. The dependence of $D(\tau = 1\text{s})$ on α and Φ follows a power-law dependence with an exponent of approximately 6 in both cases. The same functional dependence was found for n with exponents equal to 1.6 and 2.1, respectively. The similar functional dependence of $D(\tau = 1\text{s})$ and n as a function of α and Φ supports our assumption that the effects of confinement are essentially determined by the motion in the 2–3 plane. In order to better understand the origin of the average dynamical behavior in confinement, we performed a single-trajectory analysis.

3.3.2. Velocity distributions and reorientation descriptors

Instantaneous velocities were extracted from trajectory segments, calculating the ratio of the distance between two consecutive spots in a trajectory and the corresponding time difference. The mean, maximal,

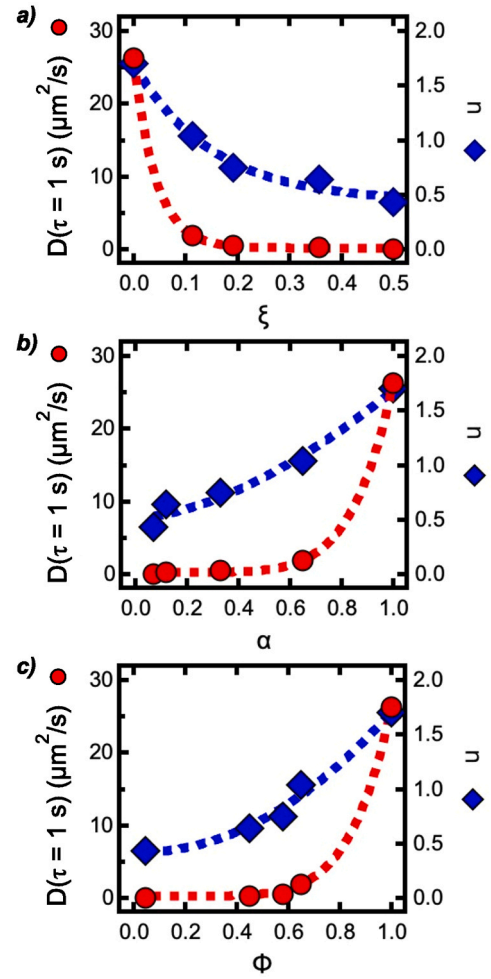


Fig. 3. $D(\tau = 1\text{s})$ and power-law exponent n of the average MSD $\langle \Delta r^2(\tau) \rangle$ as a function of the confinement length (a), the pore area fraction (b), and the pore volume fraction (c).

minimal, and median instantaneous velocities of a trajectory were calculated considering all the segments composing the trajectory. By repeating the calculation for all trajectories, we obtained the corresponding distributions. Fig. 4a reports the distributions obtained for the median velocity for different confinement conditions, similar results were obtained for the mean, max and min velocities. Changes in the median velocity distribution confirm the confinement effect of the polymer matrix on the bacterial motion. The overall distribution shifts to smaller velocities with increasing confinement (Fig. 4a); furthermore the distribution becomes narrower, suggesting an increasing control of the confining space on the bacterial velocity. The median value of the distribution (Fig. 4b) shows an approximately linear decrease with increasing confinement length ξ .

Moreover, through the analysis of single-trajectories we determined the average reorientation rate (γ), with the reorientation rate for a trajectory j defined as:

$$\gamma_j = \frac{\sum_i \theta_{i,i+1}}{N\Delta t_j} \quad (6)$$

where $\theta_{i,i+1}$ is the reorientation angle between two consecutive steps, i and $i + 1$, in a trajectory j , N is the total number of reorientation events and Δt_j is the total duration of the trajectory. The mean value γ was calculated by averaging over all trajectories. We also considered the mean straight line speed (V_{SL}^j), defined as the speed that the bacteria would present when moving at constant speed along a straight line from

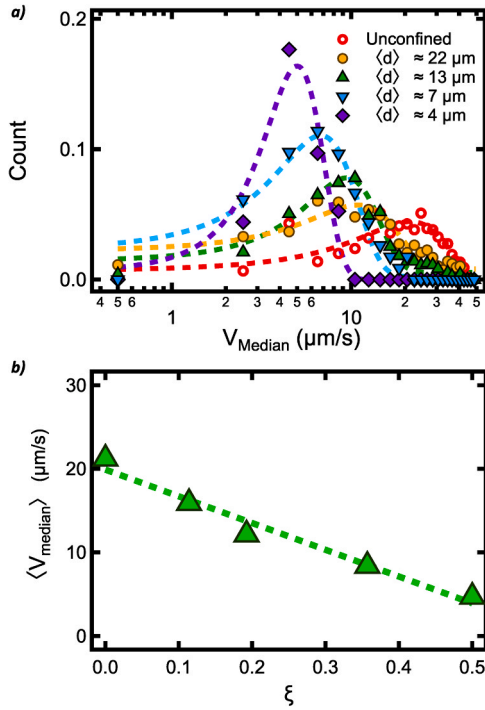


Fig. 4. (a) Distribution of the median velocity of all investigated trajectories for different confinement conditions (as indicated), and (b) median value of the distribution as a function of the confinement length ξ .

the initial to the final spot of a trajectory:

$$V_{\text{SL}}^j = \frac{d_{j0}}{\Delta t_j} \quad (7)$$

where d_{j0} is the net distance from the origin traveled in the time Δt_j for the trajectory j . The value $\langle V_{\text{SL}} \rangle$ is the average over all trajectories. We finally calculated also the confinement ratio (CR), or persistence:

$$CR = \frac{d_{j0}}{\sum_i d_{i,i+1}} \quad (8)$$

where $\sum_i d_{i,i+1}$ is the total distance traveled along a trajectory. Also this value was averaged over all trajectories.

The dependence of the three parameters on the confinement length ξ is reported in Fig. 5. Corresponding plots as a function of pore volume fraction (Φ) and pore area fraction (α) are reported in Fig. S7 of the SI. While free-diffusing bacteria show the largest mean straight line velocity

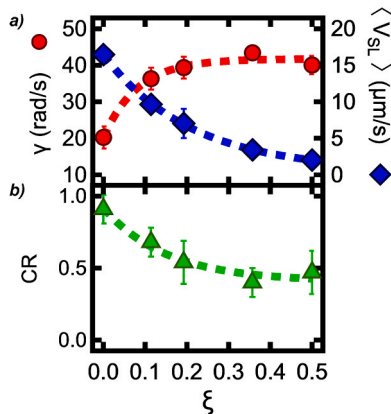


Fig. 5. Average reorientation rate γ , mean straight line velocity $\langle V_{\text{SL}} \rangle$ (a), and mean confinement ratio CR (b) as a function of the confinement length.

and the smallest average reorientation rate (Fig. 5a), the first decreases with increasing confinement while the second increases reaching an almost constant γ of ≈ 40 rad/s for $\xi > 0.2$. This plateau value is possibly a physical limit of the *B. subtilis*. Note that, compared to $\langle V_r \rangle$, $\langle V_{\text{SL}} \rangle$ decreases more rapidly as a function of confinement: this can be explained with the suppression of straight trajectories in favor of random motion typical of diffusion or sub-diffusion. The confinement ratio also confirms that the confinement induces randomization of the bacterial motion: CR ≈ 1 in the dispersion of unconfined bacteria, while it decreases to approximately 0.5 under the strongest confinement conditions (Fig. 5b). The observed trends thus indicate that with increasing confinement the bacteria can perform less and less straight trajectories typical of the run-and-tumble motion and need to reorient more often to escape the confinement imposed by the hydrogel.

3.3.3. Classification of trajectories

Trajectories were split into segments that were classified according to the following equations[65]:

$$\langle r_{(m)}^2(t) \rangle = 4Km\Delta t \quad (9)$$

for diffusion,

$$\langle r_{(m)}^2(t) \rangle = 4K(m\Delta t)^\alpha \quad (10)$$

for sub-diffusion, where $\alpha < 1$ and:

$$\langle r_{(m)}^2(t) \rangle = 4Km\Delta t + (\nu m\Delta t)^2 \quad (11)$$

for active motion, with ν the velocity parameter. In all equations, m represents the number of trajectory segments that can be classified according to the corresponding type of motion and $\langle r_{(m)}^2(t) \rangle$ the corresponding average squared displacement.

Note that in previous studies on *E. coli* [31] only a qualitative distinction between hopping and trapping events along single trajectories was discussed, without presenting a quantitative classification of trajectory segments that also distinguishes between active and diffusive motion. Fig. 6 shows the results of the classification: In the unconfined case the large majority of the trajectory segments can be classified as active motion, with a small fraction of diffusive segments, possibly associated with the end of the trajectories, where randomization of the direction appears, also explaining the $n \approx 1.7$ exponent of the MSD (instead of 2 expected for purely active motion); for increasing confinement, the percentage of active trajectory segments sharply decreases, reaching a plateau corresponding to approximately 20% of the total for $\xi > 0.2$. Note that at this value of ξ the plateau of the reorientation rate is also observed. At the same time the number of sub-diffusive trajectory segments, which were absent in the unconfined system, increases approximately linearly with ξ . On the other hand, the population of diffusive trajectory segments presents a maximum at intermediate confinement and attains also a plateau for the larger values of ξ . The results of the classification show that within each trajectory there is a coexistence of different types of motion in all confined conditions, with the average dynamics represented by the MSD that are the result of the relative fraction of trajectory segments that undergo active, diffusive or sub-diffusive motions. There are thus no clearly distinct populations of bacteria presenting active, diffusive or sub-diffusive motion, it is rather the motion of individual bacteria that contains these three different behaviors. For the strongest confinement conditions, the population of sub-diffusive trajectory segments becomes dominant, while for $0.1 \leq \xi \leq 0.2$ the 3 populations are comparable and all contribute to the overall MSD. An additional remark is that the growth of the reorientation rate coincides with the increase in the population of diffusive segments, while its plateau with the drop in the same population. This suggests that the most significant bacterial reorientation allowing to escape confinement occurs along the diffusive

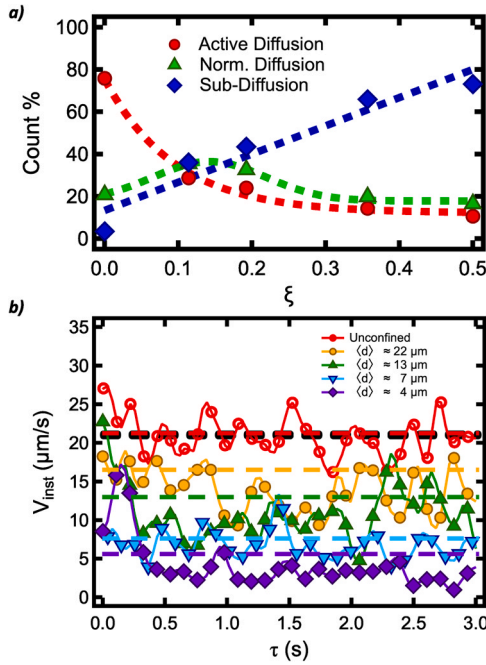


Fig. 6. (a) Normalized populations of trajectory segments classified as active, diffusive or sub-diffusive, as a function of the confining length (ξ). (b) Time evolution of the instantaneous velocities for exemplary single trajectories of bacteria swimming in unconfined conditions (empty markers), and through the different confining matrices (full markers), as indicated. For clarity, the number of markers was reduced, reporting one every 3 experimental points. Corresponding median speeds extracted from the velocity distributions of Fig. 4 are indicated by dashed lines.

segments of the trajectories.

3.3.4. Transport models

For flagella-propelled bacteria that display run-and-tumble motility characterized by ballistic runs of mean speed $\langle V_r \rangle$ and length $\langle L_r \rangle$, resulting from both the straight runs and tumbling events, at sufficiently long time randomization of the trajectories leads to diffusive motion with a diffusion coefficient given by the expression [14,66–69,70]:

$$D_{\text{RT}} \approx \frac{\langle V_r \rangle \langle L_r \rangle}{3} \quad (12)$$

For the unconfined bacteria dispersion Eq. (12) provides a value that is indeed in very good agreement with that obtained from the analysis of

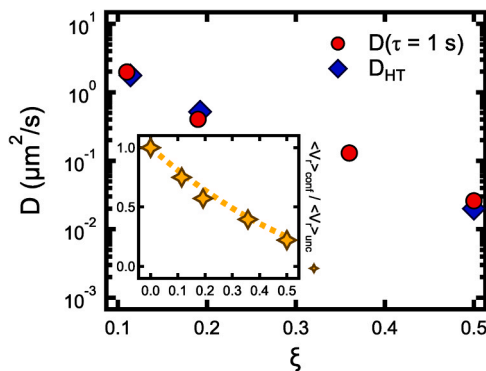


Fig. 7. Motility coefficient experimentally determined from the time and ensemble-averaged MSDs ($D(\tau = 1 \text{ s})$), and predicted from the hopping and trapping model D_{HT} (as indicated). Median running velocities normalized by the velocity in unconfined conditions as a function of the confinement length (ξ). The dashed line corresponds to the model of Eq. (14).

the MSDs (Fig. 7), even if complete randomization of the motion was not achieved in the analyzed time interval. In confinement, it has been often assumed [35,36] that the motion of the bacteria remains ballistic and is still performed at a mean run speed $\langle V_r \rangle$, but for shorter run lengths, $L'_r < L_r$, due to the pore confinement. Often L'_r has been assumed to correspond to the pore size. However, the time dependence of the MSDs, as well as the single-trajectory analysis reported in previous work on *E. coli* bacteria in soft confinement [31,34], and the single trajectory classification presented here, show that there is a qualitative change in the motion of bacteria at the single trajectory level, with trajectories that on top of active run-and-tumble motion present diffusive and sub-diffusive segments.

The studies in [31,34] proposed a different approach to estimate an effective diffusivity, in which the bacterial motion in confinement is described in terms of a series of hopping and trapping events along bacterial trajectories. The analysis presented in the previous section for our system is consistent with this picture, since it was shown that trajectory segments can be decomposed into active, diffusive, and sub-diffusive. The sub-diffusive segments can be seen as trapping periods, while diffusive and active segments as hopping events. Note that while in [31] hopping was associated only with active motion, the analysis of the reorientation rate coupled with trajectory classification suggests that in our case also diffusive displacements contribute to the escape from local trapping. To provide an expression of the effective diffusion coefficient, Battacharjee *et al.* [31] described the bacterial motion as a random walk, in which walk lengths are given by the hopping lengths L_h , since $L_h \gg L_t$, with h and t referring to hopping and trapping, respectively, while the walk times are assumed to be equal to the trapping times τ_t , since $\tau_t \gg \tau_h$. Under these assumptions:

$$D_{\text{HT}} \approx \frac{\langle L_h \rangle^2}{3 \langle \tau_t \rangle} \quad (13)$$

The detailed single-trajectory analysis allowed the differentiation of hopping and trapping events by following the time evolution of the instantaneous velocity of each bacteria along single trajectories. Consistent with the expectations, the temporal traces reported in Fig. 6 (b) exhibit the characteristic intermittent switching between ballistic or diffusive faster runs (hops), corresponding to the spikes in the temporal traces, and slower trapping periods, corresponding to the flat bottom of the temporal traces. We note that different from studies on *E. coli* [31], the spikes of instantaneous velocity in confined conditions are significantly smaller than the bulk run velocity. This confirms that hops may be a combination of active runs and diffusion for the case of *B. subtilis*. Hopping and trapping times were then defined as the periods in which bacteria move with a velocity that is larger or smaller than a threshold value. Different from [31,34], in which the threshold value was assigned as $1/2 \langle V_r \rangle$ of the unconfined case, which is somewhat arbitrary, here we defined it as the median instantaneous velocity extracted from the trajectories (data reported in Fig. 4). This choice was additionally dictated by the evidence that also diffusive motion, together with active motion, contributes to release from local entrapment. Therefore the run velocity in unconfined conditions is not representing a meaningful reference value. To determine the average hopping length for the different confinement conditions we analysed again the single segments along each trajectory and extracted those that exceed a threshold value equal to $\langle v_{\text{median}} \rangle \Delta t$, with Δt the delay time between two steps in a trajectory. By analysing all trajectories we determined the distributions of L_h (Fig. S8 of the SI) and their median value (values reported in Tab. S2 of the SI) for different confinement conditions. For $\langle d \rangle = 7 \mu\text{m}$ the distribution was found to be too noisy to properly determine the median value, therefore this value was not reported. Note that the fact that $\langle L_h \rangle$ is always smaller than the average pore size suggests the presence of bacteria-bacteria and/or bacteria-matrix interactions mediated by sensory organs, such as pili, randomly distributed on the cell membrane. As expected, the characteristic hopping length is strongly affected by the

imposed confinement, following an exponential decay with the increase of the confinement length and a roughly linear trend with the pore area and volume fraction, see Fig. S9 of the SI. The new effective diffusion coefficients D_{HT} calculated through Eq. (13) are in very good agreement with the experimental data for $D(t = 1s)$ (Fig. 7a). Note that the latter values are determined in conditions where the system does not yet display a diffusive motion, however they seem to provide a good approximation to the effective diffusion coefficient. We report in Table S3 of the SI the calculation of D_{HT} using as a reference value for distinguishing hopping events $1/2\langle V_r \rangle$ in unconfined conditions, showing that with this choice the experimental transport coefficients in confinement are strongly underestimated. Fig. S10 of the SI shows the dependence of D_{HT} on α and ϕ .

It is interesting to note that the median speed of the diffusing bacteria in confinement, $\langle V_r \rangle_{conf}$, can be related to its corresponding unconfined value, $\langle V_r \rangle_{unc}$, through ξ , as expressed in the following equation:

$$\langle V_r \rangle_{conf} = (1 - \xi)^2 \langle V_r \rangle_{unc} \quad (14)$$

The insight of Fig. 7b reports the experimentally determined median running speeds of the bacteria normalized by the speed in unconfined conditions (yellow marker) and the predicted values (dotted line) as a function of the corresponding confinement lengths; as is clearly observable the experimental values are in very good agreement with the model expressed in Eq. (14). The quantity $(1 - \xi)^2$ could be interpreted as the ratio between the area of an effective pore having a diameter $\langle d \rangle - l_{bacteria}$, $A_{free} = \pi(\langle d \rangle - l_{bacteria})^2/4$ and the corresponding average pore area $A_{pore} = \pi\langle d \rangle^2/4$.

We last analyze the normalized probability densities of trapping times $P(\tau_t)$ (Fig. 8a). These extend to increasingly longer times with decreasing pore size, indicating the progressively stronger effect of

confinement that leads to localization of the motion over increasingly longer trapping times. The probability densities can be described with a compressed exponential function:

$$P(\tau_t) \approx A \exp\left[-(\tau_t/\tau_d)^\beta\right] \quad (15)$$

in which τ_d is the characteristic time of the decay and β is the compressing exponent. We did not find previous evidences of this kind of distribution, nor theoretical models that predict this form. Typical models of anomalous diffusion in passive systems, like for example the already mentioned CTRW[61], would predict power-law tails of the trapping time distribution in the limit of long times, with $P(\tau_t) \sim \tau_t^{-1-n}$ and n the sub-diffusive exponent of the MSD. Fits of such power-law dependencies of the distributions of Fig. 8a., in the regime $P(\tau_t) < 0.4$ yield values of the power-law exponent comprised between -3.8 (larger pore diameter) and -2.6 (smaller pore diameter) that are not consistent with the values of n obtained from MSDs. The characteristic time of the decay τ_d extracted from the fits reflects the increase of the confinement both in relation to the confinement length ξ and the pore area fraction α , Fig. 8b-c respectively. Indeed it is found to increase(decrease) with increasing confinement length (pore area fraction), consistent with an increasing average trapping duration for stronger confinement. The stretching exponent β increases with increasing confinement, indicating a progressively stronger compressed exponential behavior. Compressed exponential distributions have been associated in glassy systems to avalanche like dynamics below the glass transition temperature[71]. The connection between the bacterial dynamics in confinement and avalanche-like phenomena should be investigated in the future.

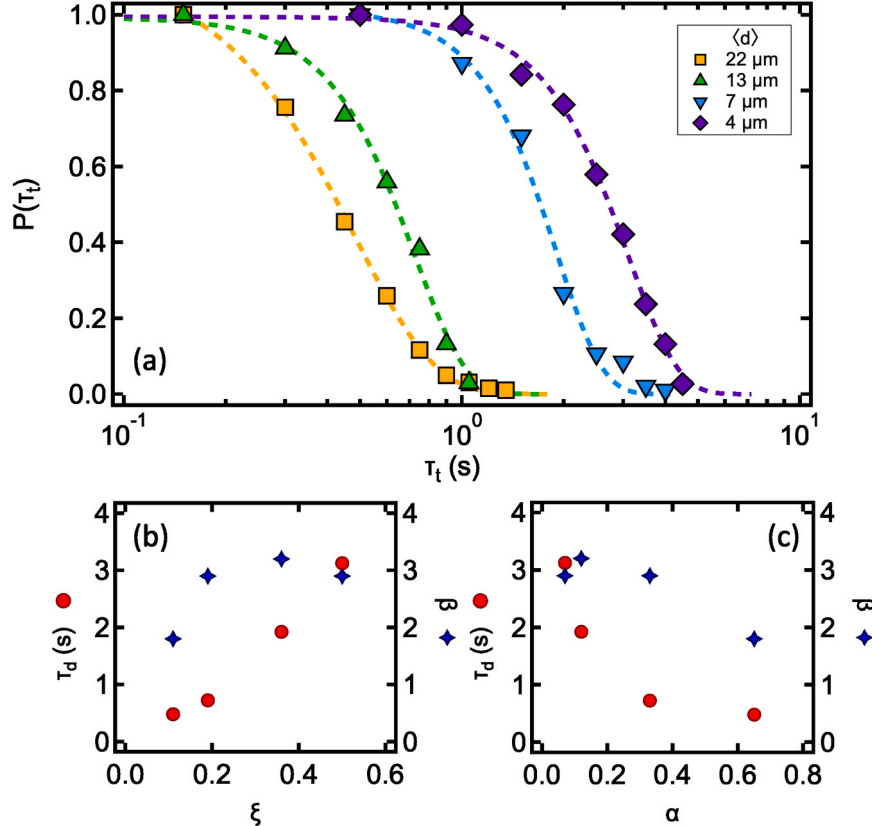


Fig. 8. (a) Probability density distributions $P(\tau_t)$ (symbols) of the trapping times τ_t in the different confining matrices, as indicated. Dashed lines represent fits to a stretched exponential function, Eq. (15). (b-c) Characteristic parameters τ_d and β resulting from the fits in (a), as a function of the confinement length (b), and the pore area fraction (c).

4. Conclusions

We investigated the effects of confinement on the motility of *B. subtilis* using biocompatible hydrogels with a high degree of transparency as model porous media mimicking typical habitats for this microorganism.

Thanks to the precise synthesis and morphological characterization of the confining porous matrix and single-trajectory analysis of bacterial motion obtained by particle tracking, a quantitative description of the dynamic behavior of the bacteria as a function of the degree of confinement was obtained. The well-known run-and-tumble motility of *B. subtilis*, resulting in a super-diffusive MSD at short times and diffusive behavior at long times, was found to be strongly affected by confinement. By decreasing the hydrogel pore size, MSDs shift from diffusive to sub-diffusive at short times. Analyzing single trajectories, we show that this transition is associated with a qualitative change in the dynamics of individual bacteria. Single trajectories in confinement present a combination of active, diffusive and subdiffusive segments. Active segments are strongly depressed in confinement and are substituted by diffusive and subdiffusive segments at intermediate confinements, while sub-diffusive segments dominate for stronger confinements. This transition is reflected in a strong reduction of the median velocity and a strong increase in the reorientational rate. The alternation of different dynamics can be described in terms of a hopping and trapping motion, with the entrapment induced by the confining porosity. While for *E. coli* release from local confinement was described in terms of active jumps with instantaneous velocity that exceeds half the run velocity in unconfined conditions, for *B. subtilis* hopping events involve both active and diffusive motions. We therefore redefined hopping events in our case in terms of displacements with an instantaneous velocity that exceeds the median velocity estimated from trajectories. Using this definition of hopping events, the transport coefficients estimated from the MSDs at long times are in good agreement with predictions of a recent model of hopping and trapping motion [31]. Finally, we introduced an empirical relation that quantitatively links the median velocity under confined and unconfined conditions via the characteristic length and the effective pore area associated to the imposed confinement.

Our results highlight the importance of combining single trajectory analysis and detailed morphological characterization of the confining matrix to understand active diffusion in highly confining media. The qualitative changes of the motility in confinement and the quantitative link to porosity presented in our study will serve as a guide for the investigation of bacterial migration and proliferation processes of microorganisms in natural confining habitats, such as soil or tissues. Additional effort will be dedicated to extend our studies to bacteria presenting different motility, and to include the effects of flow fields.

CRedit authorship contribution statement

Bassu Gavino: Conceptualization, Formal analysis, Investigation, Methodology, Software, Visualization, Writing – original draft. **Fratini Emiliano:** Conceptualization, Funding acquisition, Project administration, Resources, Supervision, Writing – review & editing. **Laurati Marco:** Conceptualization, Funding acquisition, Resources, Supervision, Validation, Writing – original draft.

Declaration of Competing Interest

The authors declare that they have no known competing financial interests or personal relationships that could have appeared to influence the work reported in this paper.

Data availability

Data will be made available on request.

Acknowledgments

This work has been supported by the Italian Ministero dell'Istruzione, dell'Università e della Ricerca through the "Progetto Dipartimenti di Eccellenza 2018–2022" granted to the Department of Chemistry "Ugo Schiff" of the University of Florence. We also thank Consorzio Interuniversitario per lo Sviluppo dei Sistemi a Grande Interfase, CSGI (Center for Colloid and Surface Science) for partial financial support. We acknowledge the biological laboratory of the Department of Chemistry at the University of Florence, and in particular Dr. S. Tilli, for lab assistance with the preparation of the bacterial cultures.

Appendix A. Supporting information

Supplementary data associated with this article can be found in the online version at doi:10.1016/j.colsurfb.2024.113797.

References

- [1] A.A. Salyers, D.D. Whitt, D.D. Whitt, *Bacterial pathogenesis: a molecular approach*, Vol. 1, ASM Press, Washington, DC, 1994.
- [2] N. Woodford, D.M. Livermore, Infections caused by gram-positive bacteria: a review of the global challenge, *J. Infect.* 59 (2009) S4–S16.
- [3] M.G. Gareau, P.M. Sherman, W.A. Walker, Probiotics and the gut microbiota in intestinal health and disease, *Nat. Rev. Gastroenterol. Hepatol.* 7 (9) (2010) 503–514.
- [4] P.P. Nagarkar, S.D. Ravetkar, M.G. Watve, Oligophilic bacteria as tools to monitor aseptic pharmaceutical production units, *Appl. Environ. Microbiol.* 67 (3) (2001) 1371–1374.
- [5] T.A. Harper, S. Bridgewater, L. Brown, P. Pow-Brown, A. Stewart-Johnson, A. Adesiyun, Bioaerosol sampling for airborne bacteria in a small animal veterinary teaching hospital, *Infect. Ecol. Epidemiol.* 3 (1) (2013) 20376.
- [6] S. Kandel, N. Herschberger, S. Kim, S. Doty, Diazotrophic endophytes of poplar and willow for growth promotion of rice plants in nitrogen-limited conditions, *Crop Sci.* 55 (4) (2015) 1765–1772.
- [7] Y. Asada, J. Miyake, Photobiological hydrogen production, *J. Biosci. Bioeng.* 88 (1) (1999) 1–6.
- [8] A. Esmaeili, A.A. Pourbabae, H.A. Alikhani, F. Shabani, E. Esmaeili, Biodegradation of low-density polyethylene (ldpe) by mixed culture of *lysiniabacillus xylanilyticus* and *aspergillus niger* in soil, *Plos One* 8 (9) (2013) e71720.
- [9] O. Habimana, A. Semião, E. Casey, The role of cell-surface interactions in bacterial initial adhesion and consequent biofilm formation on nanofiltration/reverse osmosis membranes, *J. Membr. Sci.* 454 (2014) 82–96.
- [10] K.F. Jarrell, M.J. McBride, The surprisingly diverse ways that prokaryotes move, *Nat. Rev. Microbiol.* 6 (6) (2008) 466–476.
- [11] A. Bren, M. Eisenbach, How signals are heard during bacterial chemotaxis: protein-protein interactions in sensory signal propagation, *J. Bacteriol.* 182 (24) (2000) 6865–6873.
- [12] R.M. Harshey, Bacterial motility on a surface: many ways to a common goal, *Annu. Rev. Microbiol.* 57 (2003) 249.
- [13] E. Lauga, Bacterial hydrodynamics, *Annu. Rev. Fluid Mech.* 48 (2016) 105–130.
- [14] H.C. Berg, Random walks in biology, in: *Random Walks in Biology*, Princeton University Press, 2018.
- [15] N. Wadhwa, H.C. Berg, Bacterial motility: machinery and mechanisms, *Nat. Rev. Microbiol.* 20 (3) (2022) 161–173, <https://doi.org/10.1038/s41579-021-00626-4>.
- [16] L. Lemelle, J.-F. Paliere, E. Chatre, C. Place, Counterclockwise circular motion of bacteria swimming at the air-liquid interface, *J. Bacteriol.* 192 (23) (2010) 6307–6308.
- [17] D. Giaché, T. Ishikawa, T. Yamaguchi, Hydrodynamic entrapment of bacteria swimming near a solid surface, *Phys. Rev. E* 82 (5) (2010) 056309.
- [18] K. Drescher, J. Dunkel, L.H. Cisneros, S. Ganguly, R.E. Goldstein, Fluid dynamics and noise in bacterial cell-cell and cell-surface scattering, *Proc. Natl. Acad. Sci.* 108 (27) (2011) 10940–10945.
- [19] J. Elgeti, G. Gompper, Self-propelled rods near surfaces, *Europhys. Lett.* 85 (3) (2009) 38002, <https://doi.org/10.1209/0295-5075/85/38002>.
- [20] G. Li, J.X. Tang, Accumulation of microswimmers near a surface mediated by collision and rotational brownian motion, *Phys. Rev. Lett.* 103 (2009) 078101, <https://doi.org/10.1103/PhysRevLett.103.078101>.
- [21] G. Junot, T. Darnige, A. Lindner, V.A. Martinez, J. Arlt, A. Dawson, W.C.K. Poon, H. Auradou, E. Clément, Run-to-tumble variability controls the surface residence times of *e. coli* bacteria, *Phys. Rev. Lett.* 128 (2022) 248101, <https://doi.org/10.1103/PhysRevLett.128.248101>.
- [22] J. Männik, R. Driessen, P. Galajda, J. Keymer, C. Dekker, Bacterial growth and motility in sub-micron constrictions, *Proc. Natl. Acad. Sci. USA* 106 (2009) 14861–14866, <https://doi.org/10.1073/pnas.0907542106>.
- [23] M. Binz, A.P. Lee, C. Edwards, D.V. Nicolau, Motility of bacteria in microfluidic structures, *Microelectron. Eng.* 87 (5-8) (2010) 810–813.

- [24] B. Libberton, M. Binz, H. Van Zalinge, D.V. Nicolau, Efficiency of the flagellar propulsion of *Escherichia coli* in confined microfluidic geometries, *Phys. Rev. E* 99 (1) (2019) 012408.
- [25] V. Tokárová, A. Sudalayadum Perumal, M. Nayak, H. Shum, O. Kašpar, K. Rajendran, M. Mohammadi, C. Tremblay, E.A. Gaffney, S. Martel, D.V. Nicolau, D.V. Nicolau, Patterns of bacterial motility in microfluidics-confining environments, *Proc. Natl. Acad. Sci.* 118 (17) (2021) 1–12, <https://doi.org/10.1073/pnas.2013925118>.
- [26] A. Dehkharghani, N. Waisbord, J.S. Guasto, Self-transport of swimming bacteria is impaired by porous microstructure, *Commun. Phys.* 6 (1) (2023) 18, <https://doi.org/10.1038/s42005-023-01136-w>.
- [27] R.M. Ford, R.W. Harvey, Role of chemotaxis in the transport of bacteria through saturated porous media (biological processes in porous media: From the pore scale to the field), *Adv. Water Resour.* 30 (6) (2007) 1608–1617, <https://doi.org/10.1016/j.advwatres.2006.05.019>, (<https://www.sciencedirect.com/science/article/pii/S0309170806001382>) (biological processes in porous media: From the pore scale to the field).
- [28] T. Bertrand, Y. Zhao, O. Bénichou, J. Tailleur, R. Voituriez, Optimized diffusion of run-and-tumble particles in crowded environments, *Phys. Rev. Lett.* 120 (2018) 198103, <https://doi.org/10.1103/PhysRevLett.120.198103>.
- [29] T. Jakuszeit, O.A. Croze, S. Bell, Diffusion of active particles in a complex environment: role of surface scattering, *Phys. Rev. E* 99 (2019) 012610, <https://doi.org/10.1103/PhysRevE.99.012610>.
- [30] A. Morin, N. Desreumaux, J.-B. Caussin, D. Bartolo, Distortion and destruction of colloidal flocks in disordered environments, *Nat. Phys.* 13 (1) (2017) 63–67, <https://doi.org/10.1038/nphys3903>.
- [31] T. Bhattacharjee, S.S. Datta, Bacterial hopping and trapping in porous media, *Nat. Commun.* 10 (1) (2019) 2–10, <https://doi.org/10.1038/s41467-019-10115-1>.
- [32] Y. wei Liu, P. Wang, J. Wang, B. Xu, J. Xu, J. gang Yuan, Y. yuan Yu, Q. Wang, Transparent and tough poly(2-hydroxyethyl methacrylate) hydrogels prepared in water/IL mixtures, *N. J. Chem.* 44 (10) (2020) 4092–4098, <https://doi.org/10.1039/d0nj00214c>.
- [33] G. Bassu, M. Laurati, E. Fratini, Microgel dynamics within the 3d porous structure of transparent peg hydrogels, *Colloids Surf. B: Biointerfaces* 221 (2023) 112938.
- [34] T. Bhattacharjee, S.S. Datta, Confinement and activity regulate bacterial motion in porous media, *Soft Matter* 15 (48) (2019) 9920–9930, <https://doi.org/10.1039/c9sm01735f>.
- [35] D. Lauffenburger, C.R. Kennedy, R. Aris, Traveling bands of chemotactic bacteria in the context of population growth, *Bull. Math. Biol.* 46 (1) (1984) 19–40.
- [36] N.A. Licata, B. Mohari, C. Fuqua, S. Setayeshgar, Diffusion of bacterial cells in porous media, *Biophys. J.* 110 (1) (2016) 247–257.
- [37] Y. Su, C. Liu, H. Fang, D. Zhang, *Bacillus subtilis*: A universal cell factory for industry, agriculture, biomaterials and medicine, *Microb. Cell Factor.* 19 (1) (2020) 1–12, <https://doi.org/10.1186/s12934-020-01436-8>.
- [38] J. Chen, Y. Zhu, G. Fu, Y. Song, Z. Jin, Y. Sun, D. Zhang, High-level intra-and extra-cellular production of d-psicose 3-epimerase via a modified xylose-inducible expression system in *Bacillus subtilis*, *J. Ind. Microbiol. Biotechnol.* 43 (11) (2016) 1577–1591.
- [39] E. Aslankoobi, M.N. Rezaei, Y. Vervoort, C.M. Courtin, K.J. Verstrepen, Glycerol production by fermenting yeast cells is essential for optimal bread dough fermentation, *PLoS One* 10 (3) (2015) e0119364.
- [40] M. Ongena, P. Jacques, *Bacillus* lipopeptides: versatile weapons for plant disease biocontrol, *Trends Microbiol.* 16 (3) (2008) 115–125.
- [41] T. Pisithkul, J.W. Schroeder, E.A. Trujillo, P. Yeesin, D.M. Stevenson, T. Chaiamarit, J.J. Coon, J.D. Wang, D. Amador-Noguez, Metabolic remodeling during biofilm development of *Bacillus subtilis*, *MBio* 10 (3) (2019) e00623–19.
- [42] J. Huang, S. Liu, C. Zhang, X. Wang, J. Pu, F. Ba, S. Xue, H. Ye, T. Zhao, K. Li, et al., Programmable and printable *Bacillus subtilis* biofilms as engineered living materials, *Nat. Chem. Biol.* 15 (1) (2019) 34–41.
- [43] M. Duan, Y. Zhang, B. Zhou, Z. Qin, J. Wu, Q. Wang, Y. Yin, Effects of *Bacillus subtilis* on carbon components and microbial functional metabolism during cow manure–straw composting, *Bioresour. Technol.* 303 (2020) 122868.
- [44] R. Rusconi, J.S. Guasto, R. Stocker, Bacterial transport suppressed by fluid shear, *Nat. Phys.* 10 (3) (2014) 212–217.
- [45] P. Piggot, *Bacillus Subtilis* (2009). 10.1016/B978-012373944-5.00036-5.
- [46] A.R. Bate, R. Bonneau, P. Eichenberger, *Bacillus subtilis* systems biology: applications of-omics techniques to the study of endospore formation, *Bact. Spore.: Mol. Syst.* (2016) 129–144.
- [47] S. Gao, H. Wu, X. Yu, L. Qian, X. Gao, Swarming motility plays the major role in migration during tomato root colonization by *Bacillus subtilis* swr01, *Biol. Control* 98 (2016) 11–17.
- [48] S. Ali, M.L. Cuchiara, J.L. West. Micropatterning of poly(ethylene glycol) diacrylate hydrogels, First Ed., Elsevier Inc., 2014 <https://doi.org/10.1016/B978-0-12-800281-0.00008-7>. Vol. 121.
- [49] D. Legland, I. Arganda-Carreras, P. Andrey, MorphoLib J: integrated library and plugins for mathematical morphology with ImageJ, *Bioinformatics* 32 (22) (2016) 3532–3534, <https://doi.org/10.1093/bioinformatics/btw413>.
- [50] D.B. Allan, T. Caswell, N.C. Keim, C.M. van der Wel, R.W. Verweij, Soft-matter/trackpy: Trackpy.10.5281/zenodo.4682814.
- [51] J.C. Crocker, D.G. Grier, Methods of digital video microscopy for colloidal studies, *J. Colloid Interface Sci.* 179 (1) (1996) 298–310, <https://doi.org/10.1006/jcis.1996.0217>. (<https://linkinghub.elsevier.com/retrieve/pii/S0021979796902179>).
- [52] T. Ershov, A. Kroll, C.R. Haramagatti, H.G. Lipinski, M. Wiemann, Classification and segmentation of nanoparticle diffusion trajectories in cellular micro environments, *PLoS ONE* 12 (1) (2017) 1–20, <https://doi.org/10.1371/journal.pone.0170165>.
- [53] J.-Y. Tinevez, N. Perry, J. Schindelin, G.M. Hoopes, G.D. Reynolds, E. Laplantine, S. Y. Bednarek, S.L. Shorte, K.W. Eliceiri, TrackMate: an open and extensible platform for single-particle tracking, *Methods* 115 (2016) 80–90, <https://doi.org/10.1016/j.ymeth.2016.09.016>. (<https://linkinghub.elsevier.com/retrieve/pii/S1046202316303346>).
- [54] D. Ershov, M.-s. Phan, J.W. Pylvänäinen, S.U. Rigaud, L.L. Blanc, J.R.W. Conway, R.F. Laine, N.H. Roy, D. Bonazzi, G. Duménil, G. Jacquemet, J.-y. Tinevez, Bringing TrackMate into the era of (2021)9-12.10.1101/2021.09.03.458852.
- [55] K. Jaqaman, D. Loerke, M. Mettlen, H. Stein, S. Schmid and G. Danuser, *Nat. Methods* 5 (2008) 695–702.
- [56] H. Nishihara, S.R. Mukai, D. Yamashita, H. Tamon, Ordered Macroporous Silica by Ice Templating, *Chem. Mater.* 17 (3) (2005) 683–689, <https://doi.org/10.1021/cm048725f>.
- [57] G. Shao, D.A.H. Hanaor, X. Shen, A. Gurlo, Freeze casting: from low-dimensional building blocks to aligned porous structures—a review of novel materials, methods, and applications, *Adv. Mater. (Deerfield Beach, Fla.)* 32 (17) (2020) e1907176, <https://doi.org/10.1002/adma.201907176>. (<http://www.ncbi.nlm.nih.gov/pubmed/32163660>).
- [58] D.B. Kearns, R. Losick, Swarming motility in undomesticated *Bacillus subtilis*, *Mol. Microbiol.* 49 (3) (2003) 581–590.
- [59] A. Creppy, E. Clément, C. Douarache, M.V. D'Angelo, H. Auradou, Effect of motility on the transport of bacteria populations through a porous medium, arXiv: 1802.01879, *Phys. Rev. Fluids* 4 (1) (2019) 1–16, <https://doi.org/10.1103/PhysRevFluids.4.013102>.
- [60] G. Ariel, A. Rabani, S. Benisty, J.D. Partridge, R.M. Harshey, A. Be'Er, Swarming bacteria migrate by Lévy walk, *Nat. Commun.* 6 (1) (2015) 1–6.
- [61] F. Höfling, T. Franosch, Anomalous transport in the crowded world of biological cells, *Rep. Prog. Phys.* 76 (4) (2013) 046602, <https://doi.org/10.1088/0034-4885/76/4/046602>.
- [62] J.-H. Jeon, A.V. Chechkin, R. Metzler, Scaled brownian motion: a paradoxical process with a time dependent diffusivity for the description of anomalous diffusion, *Phys. Chem. Chem. Phys.* 16 (2014) 15811–15817, <https://doi.org/10.1039/C4CP02019G>.
- [63] J.C. Conrad, R. Poling-Skutvik, Confined flow: consequences and implications for bacteria and biofilms, *Annu. Rev. Chem. Biomol. Eng.* 9 (2018) 175–200.
- [64] J. Guan, B. Wang, S. Granick, Even hard-sphere colloidal suspensions display fickle non-gaussian diffusion, *ACS Nano* 8 (4) (2014) 3331–3336, <https://doi.org/10.1021/nn405476t>.
- [65] C.R. Haramagatti, F.H. Schacher, A.H. Müller, J. Köhler, Diblock copolymer membranes investigated by single-particle tracking, *Phys. Chem. Chem. Phys.* 13 (6) (2011) 2278–2284.
- [66] A. Baumgärtner, M. Muthukumar, A trapped polymer chain in random porous media, *J. Chem. Phys.* 87 (5) (1987) 3082–3088.
- [67] M. Muthukumar, A. Baumgärtner, Effects of entropic barriers on polymer dynamics, *Macromolecules* 22 (4) (1989) 1937–1941.
- [68] A. Villa-Torrealba, C. Chávez-Raby, P. de Castro, R. Soto, Run-and-tumble bacteria slowly approaching the diffusive regime, *Phys. Rev. E* 101 (6) (2020) 062607.
- [69] J. Han, S. Turner, H.G. Craighead, Entropic trapping and escape of long dna molecules at submicron size constriction, *Phys. Rev. Lett.* 83 (8) (1999) 1688.
- [70] M. Muthukumar, A. Baumgärtner, Diffusion of a polymer chain in random media, *Macromolecules* 22 (4) (1989) 1941–1946.
- [71] K. Trachenko, A. Zaccone, Slow stretched-exponential and fast compressed-exponential relaxation from local event dynamics, *J. Phys.: Condens. Matter* 33 (31) (2021) 315101, <https://doi.org/10.1088/1361-648X/ac04cd>.